

## Label-free Super-Resolution Microvessel Color Flow Imaging with Ultrasound

Zhengchang Kou, Junhang Zhang, Chen Gong, Jie Ji, Nathiya Vaithiyalingam Chandra Sekaran, Zikai Wang, Rita J. Miller, Yaoheng Yang, Daniel Adolfo Llano, Qifa Zhou and Michael L. Oelze

**We present phase subtraction imaging (PSI), a new spatial-temporal beamforming method that enables micrometer level resolution imaging of microvessels in live animals without labels, which are microbubbles in ultrasound super-resolution imaging. Subtraction of relative phase differences between consecutive frames beamformed with mismatched apodizations is used in PSI to overcome the diffraction limit. We validated this method by imaging both the mouse brain and rabbit kidney using different ultrasound probes and scanning machines.**

Super-resolution ultrasound imaging (SRUI) has been extensively studied in the past decade as an emerging *in vivo* microscopic imaging method that provides a unique combination of micrometer level resolution, millimeter-centimeter level penetration, and centimeter level field-of-view with the help of microbubbles. To enable precise microbubble localization and tracking, which is crucial to achieve extraordinary image resolution, a low concentration of microbubbles and a long acquisition time are common practices in the prevailing super-resolution ultrasound imaging method, i.e., ultrasound localization microscopy (ULM) [1].

Instead of relying on the outstanding signal to noise ratio (SNR) provided by the backscatter signal from microbubbles and their separability, label-free SRUI methods that could provide a resolution better than the diffraction limit relying on the native blood flow signal have also been developed with compressed sensing [2] or erythrocyte detection [3][4]. However, short acquisition and simple post-processing remain elusive in label-free SRUI. These factors strongly limit the usage of SRUI in neuroscience imaging tasks that demand high resolution in both spatial and temporal domain and clinical imaging scenarios that require fast preparation and delivery of real-time results.

We overcome the limitations of current SRUI imaging methods and achieve micrometer level resolution using both short acquisition time and a simple post-processing algorithm using a purely receive beamforming method. In addition to providing micrometer level resolution structural information of microvessels, the proposed method also provides micrometer level resolution direction and relative speed information extracted from the relative phase change resulting from the Doppler effects generated by the native blood flow.

Ultrafast ultrasound was used to acquire thousands of frames that are coherently compounded with different steering angles on the transmission within several seconds. After acquiring ultrafast ultrasound data, we performed beamforming to reconstruct

ultrasound images from the raw channel data. A brief illustration of ultrasound beamforming process is shown in Fig.1a. In the traditional beamforming process, apodization weights such as Hann window are used to reduce the sidelobe levels. Instead of beamforming with only one apodization weight, we used three apodization weights (zero-mean, dc-offset-1, and dc-offset-2) that are used in the null subtraction imaging (NSI) [5,6]. After beamforming all the acquired frames using three sets of apodizations, tissue clutter filtering was performed to remove the static tissue signal and keep the native blood flow signal that resides in a higher frequency than static tissue in the slow time direction. Three data points that resulted from the beamforming using three apodization weights are generated for each voxel as illustrated in Fig. 1b.

The phase subtraction imaging (PSI) was then performed by subtracting two precursors that were both generated by the summation of two angles as shown in Fig. 1c. For precursor A, the first angle was calculated by calculating the relative phase difference between two consecutive frames that are beamformed with one dc-offset apodization weight and the other dc-offset apodization weight. The second angle was calculated by interchanging two dc-offset apodization weights. For precursor B, the first angle was calculated by calculating the relative phase difference between two consecutive frames that are beamformed with one dc-offset apodization weight and the zero-mean apodization weight. The second angle was estimated by calculating the relative phase difference between two consecutive frames that are beamformed with the other dc-offset apodization weight and the zero-mean apodization weight. Example images of both precursors and PSI are shown in Fig.1d. The relative phase angle between two consecutive frames that were beamformed using rectangle apodization was also calculated as color flow imaging (CFI), which is also shown in Fig.1d. It can be observed that the mainlobe of PSI is much narrower than traditional CFI.

We validated PSI against conventional CFI by scanning a mouse brain (with the skull removed) using a 50-MHz ultrasound probe. High-frequency ultrasound was used to boost the SNR of the native blood flow signal because of Rayleigh scattering. Two mice were scanned and one of them had half its brain damaged due to the craniotomy. 7,500 frames were scanned in 10 seconds for each imaging plane and 70 planes were scanned to construct a volume. A comparison between PSI and CFI on the brain damaged mouse is shown in Fig. 1e. and Fig. 1f. Another comparison between PSI and CFI on the normal mouse is shown in Fig. 1g. and Fig. 1h. To have a localized view of the performance difference, we first performed cross sectional comparisons between PSI and CFI on manually selected microvessels that are shown in Fig. 1i. We then analyzed the resolution performance of PSI with two measurements. The first measurement is the microvessel radius distribution enabled by auto skeletonization. The second measurement is the global spatial frequency coverage ratio between PSI and CFI.

To further validate the performance of PSI in a lower frequency, we also scanned mouse brains with 40-MHz and 30-MHz ultrasound with the skull removed. The 30-MHz ultrasound scan was performed with an older scanning machine that could not support frequency higher than 30-MHz. To boost sensitivity and image the full depth of the mouse brain, 4,000 frames were acquired in 5.0 seconds continuously for each imaging plane in the 40-MHz scan. A comparison between PSI and CFI with 40-MHz ultrasound is shown in Fig. 2a. and Fig. 2b. The corresponding improvement ratio of spatial frequency coverage is shown in Fig. 2c. Two mouse brains were scanned with 30-MHz ultrasound. 1,920 frames were acquired in 2.4 seconds for each imaging plane, and the corresponding results are shown in Fig. 2d to Fig. 2i.

To investigate the performance of PSI in a more clinically feasible scenario, a much shorter acquisition, which was only 162 milliseconds long, was performed on a rabbit kidney using pulse inversion ultrasound (10 MHz transmit and 20 MHz receive) on a lower frequency scanning machine. Motion correction was not performed as the acquisition duration was short. The comparison between PSI and CFI is shown in Fig. 2j. and Fig. 2k.

We demonstrated the performance of PSI in label-free microvessel imaging with different frequencies of ultrasound and animal models. *In vivo* label-free super-resolution imaging with ultrasound was achieved with a beamforming only method for the first time. Depending on the animal model and ultrasound probes, up to 7x resolution improvement has been observed with PSI over CFI. The beamforming processing of PSI is composed of applying apodizations and relative phase angle calculations, which is inexpensive in computational cost. As beamforming is a global processing and there is no spatiotemporal dependency which limits the parallelization of tracking-based methods, highly parallelized processing in a GPU or FPGA could be applied to PSI to potentially enable real-time imaging [7]. The short acquisition time needed by PSI also makes it a potential choice for label-free super-resolution functional ultrasound imaging. However, like other label-free microvessel imaging technologies, PSI is also limited by the SNR from the backscatter signal of native blood flow. Therefore, the intact skull imaging is not feasible for PSI as the skull will block most of the ultrasound signal.

For clinical applications that require handheld probe scanning on patients, long acquisition is not feasible, and motion correction can fail due to out-of-plane motion. PSI can be a potential solution as the acquisition can be as short as 200 milliseconds or less to alleviate the need for motion correction.

- [1] Errico, Claudia, et al. "Ultrafast ultrasound localization microscopy for deep super-resolution vascular imaging." *Nature* 527.7579 (2015): 499-502.
- [2] Bar-Zion, Avinoam, et al. "Doppler slicing for ultrasound super-resolution without contrast agents." *BioRxiv* (2021): 2021-11.
- [3] Jensen, Jørgen Arendt, et al. "Super resolution ultrasound imaging using the erythrocytes: I: Density images." *IEEE Transactions on Ultrasonics, Ferroelectrics, and Frequency Control* (2024).
- [4] Naji, Mostafa Amin, et al. "Super Resolution Ultrasound Imaging Using the Erythrocytes: II: Velocity Images." *IEEE Transactions on Ultrasonics, Ferroelectrics, and Frequency Control* (2024).
- [5] Kou, Zhengchang, et al. "High-resolution power Doppler using null subtraction imaging." *IEEE transactions on medical imaging* 43.9 (2024): 3060-3071.
- [6] Agarwal, Anil, et al. "Improving spatial resolution using incoherent subtraction of receive beams having different apodizations." *IEEE transactions on ultrasonics, ferroelectrics, and frequency control* 66.1 (2018): 5-17.
- [7] Kou, Zhengchang, et al. "High-level synthesis design of scalable ultrafast ultrasound beamformer with single FPGA." *IEEE transactions on biomedical circuits and systems* 17.3 (2023): 446-457.

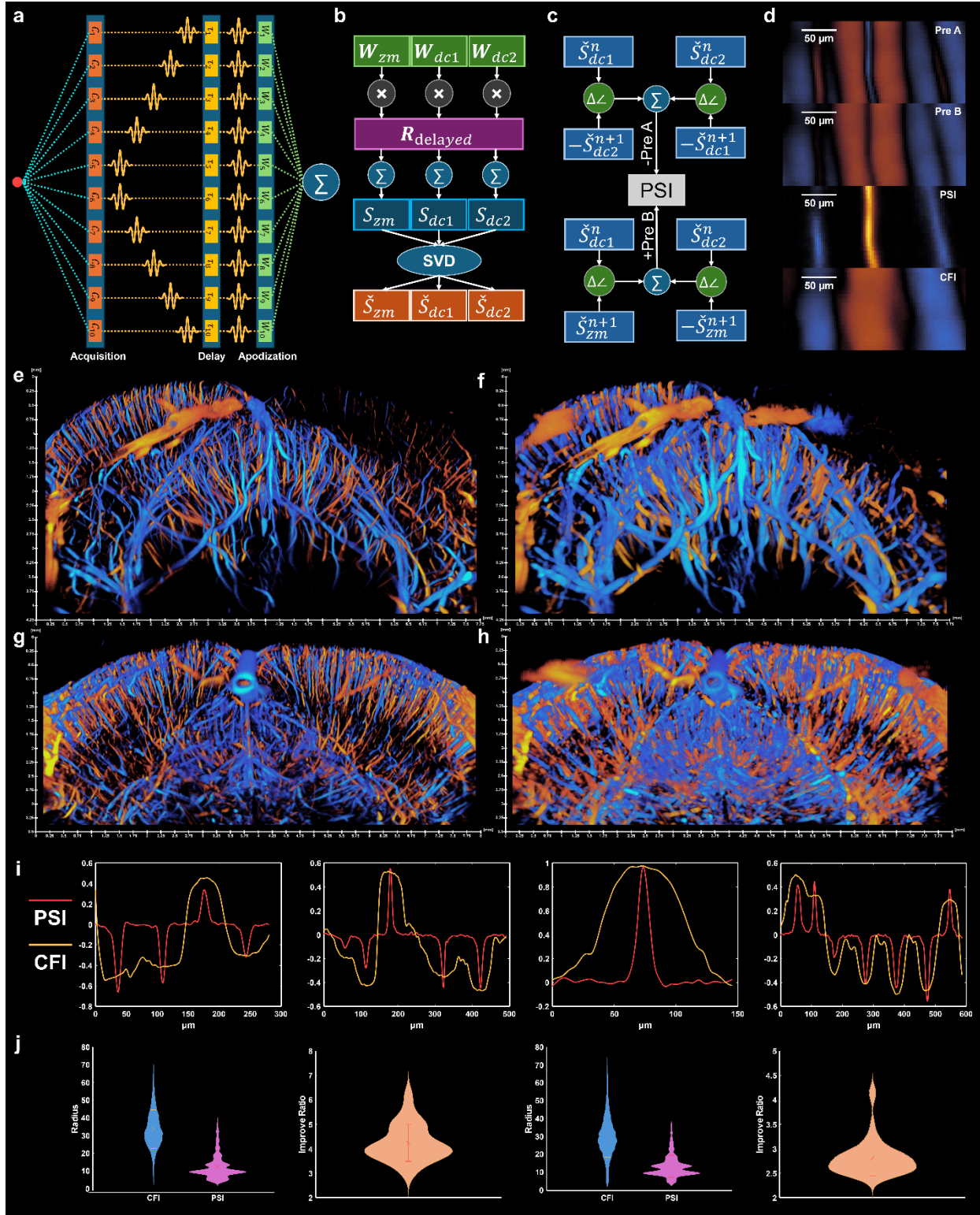


**Fig. 1 Label-free super-resolution ultrasound imaging process and label-free 50 MHz ultrasound results.** a. Block diagrams for ultrasound beamforming process which is composed of time delay compensation, apodization, and summation. b. Beamforming

and clutter filtering process of PSI. c. Phase detection and subtraction process of PSI. d. Example images of PSI and CFI along with PSI's two precursors. e. 3D PSI volume of mouse brain having brain damage on one side using 50 MHz. f. 3D CFI volume of mouse brain using having brain damage on one side 50 MHz. g. 3D CFI volume of mouse brain using 50 MHz. h. 3D CFI volume of mouse brain using 50 MHz. i. Comparison between cross sections using PSI and CFI. j. Microvessel radius distribution comparison between PSI and CFI and the global spatial frequency coverage improvement of PSI over CFI from the mouse having brain damage on one side and the normal mouse.



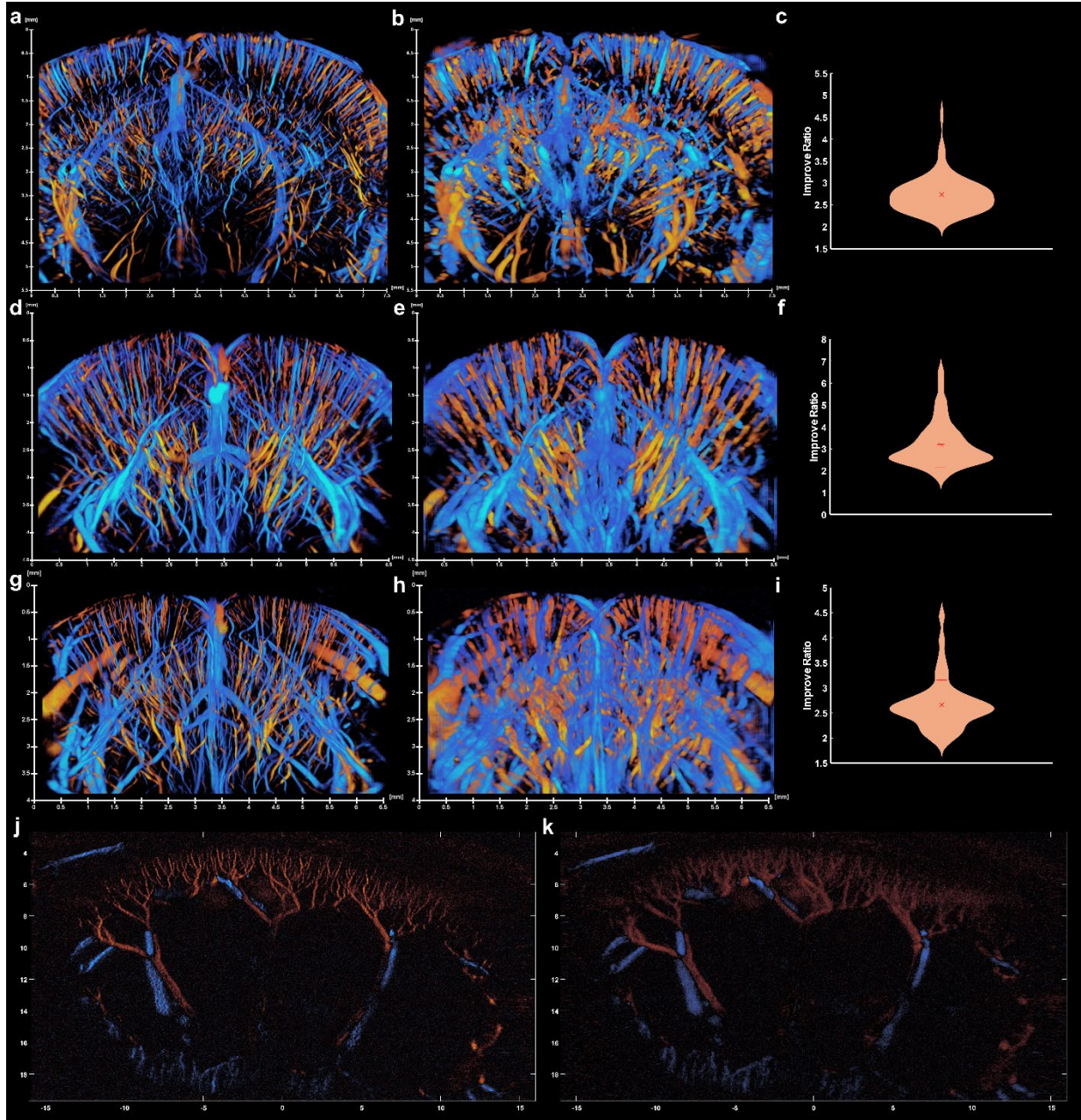


**Fig. 2 Label-free super-resolution ultrasound image of mice brain using 40 and 30 MHz ultrasound and rabbit kidney using 20 MHz ultrasound.** a-b. 3D volume rendering of mouse brain using 40 MHz ultrasound with PSI and CFI. d-e. 3D volume rendering of mouse brain using 30 MHz ultrasound with PSI and CFI. g-h. 3D volume rendering of mouse brain using 30 MHz ultrasound with PSI and CFI. j-k. 2D slice of rabbit kidney using 10 MHz on transmit and 20 MHz on receive pulse inversion ultrasound with PSI and CFI.

## METHODS

### Animal preparation.

**50M/30M Mouse:** A 2-month-old C57BL/6J mouse was anesthetized with 5% isoflurane for induction and maintained under 2% isoflurane via a nose cone. Anesthesia depth was monitored via pedal reflex and respiratory rate. To prevent corneal dehydration, GenTeal® Tears Lubricant Eye Gel (Alcon, Fort Worth, TX, USA) was applied to both eyes. The animal was positioned on a temperature-controlled heating pad throughout the procedure. The craniotomy was performed with a lateral width of 6 mm and an anterior-posterior extent from bregma to lambda. The exposed brain surface was covered with ultrasound gel to ensure acoustic coupling. All experimental procedures were approved by the Institutional Animal Care and Use Committee at the University of Southern California.

**40M Mouse:** Mouse anesthesia was induced using ketamine/xylazine anesthetics, and then mice were placed in a stereotaxic frame with a nose cone supplying oxygen for maintenance. Lidocaine (1%) was intradermally injected into the scalp to supplement anesthesia. Ear bars were used to secure the mouse head to the stereotaxic imaging stage. The scalp of the mouse was removed, and a cranial window was opened on the left and right sides of the skull using a rotary Dremel tool, starting at the sagittal suture and moving laterally to expose the lateral expanse of the cerebral cortex. The animal use protocol was approved by the Institutional Animal Care and Use Committee at the University of Illinois at Urbana-Champaign.

**Rabbit:** One *in vivo* trial was performed with a 3.5-month-old female New Zealand White rabbit weighing 5.8 kg (Charles River Laboratories, Wilmington, MA). The animal use protocol was approved by the Institutional Animal Care and Use Committee at the University of Illinois at Urbana-Champaign. Anesthesia was induced with 5% isoflurane and maintained with 2% isoflurane, both via face mask. The level of anesthesia was monitored by pedal reflex and respiratory rate. Ophthalmic ointment was applied bilaterally, and the rabbit was placed on a heating pad to maintain body temperature. The skin over the left kidney was shaved. The left kidney was scanned transabdominally by handheld VisualSonics MS200 probe.

**Ultrafast ultrasound.** Ultrafast ultrasound data were acquired using commercialized ultrasound imaging research systems and ultrasound linear arrays without modification in hardware.

**50 MHz mouse brain imaging:** A Verasonics NXT 256 high-frequency configuration ultrasound imaging research platform that has 256 channels was used with a VisualSonics MS700 linear array that has 256 elements and a center frequency of 50 MHz. The center 224 elements (total width = 8.2 mm) of the probe were used. An ultrafast plane-wave imaging sequence (19 titled plane waves,  $-9^{\circ}$  to  $9^{\circ}$  in  $1^{\circ}$  step size, pulse-



repetition frequency PRF=14,250 Hz) was developed to acquire ultrafast ultrasound data at a compounded frame rate of 750 Hz. A 50-MHz, 1.5 cycle pulse was generated by the ultrasound system as the transmit signal. Each acquisition has 768 16-bit quantization samples in fast time with a sampling frequency of 125 MHz. The ultrasound data were transferred to a host computer (Dell Precision 7960 with Intel Xeon W7-3565X and 512 GB DDR5 RAM) via PCI-Express Gen3 x16 interface and stored to a NVME SSD array (RAID 0 with 4x Samsung 990 Pro 4TB). 5 sets of 1,500 compounded frames were acquired for each imaging plane (10 seconds acquisition for each imaging plane) to enhance signal to noise ratio (SNR). The imaging array was fixed on a motorized stage to translate in elevational direction with a step size of 63.5  $\mu\text{m}$ .

40 MHz mouse brain imaging: A Verasonics NXT 256 high-frequency configuration ultrasound imaging research platform that has 256 channels was used with a VisualSonics MS550S linear array that has 256 elements and a center frequency of 40 MHz. The center 160 elements (total width = 8.4 mm) of the probe were used. An ultrafast plane-wave imaging sequence (15 titled plane waves,  $-7^\circ$  to  $7^\circ$  in  $1^\circ$  step size, pulse-repetition frequency PRF=12,000 Hz) was developed to acquire ultrafast ultrasound data at a compounded frame rate of 800 Hz. A 41.67-MHz, 1.5 cycle pulse was generated by the ultrasound system as the transmit signal. Each acquisition has 1024 16-bit quantization samples in fast time with a sampling frequency of 125 MHz. The ultrasound data were transferred to a host computer (Dell Precision 5860 with Intel Xeon W7-2595X and 256 GB DDR5 RAM) via PCI-Express Gen3 x16 interface and stored to a NVME SSD array (RAID 0 with 8x Samsung 990 Pro 2TB). 4,000 compounded frames were acquired for each imaging plane (5 seconds acquisition for each imaging plane) to enhance the sensitivity to deeper vessels. The imaging array was fixed on a motorized stage to translate in elevational direction with a step size of 50  $\mu\text{m}$ .

30 MHz mouse brain imaging: A Verasonics Vantage 256 high-frequency configuration ultrasound imaging research platform that has 256 channels was used with a VisualSonics MS550D linear array that has 256 elements and a center frequency of 40 MHz. The center 128 elements (total width = 6.8 mm) of the probe were used. An ultrafast plane-wave imaging sequence (9 titled plane waves,  $-18^\circ$  to  $18^\circ$  in  $4.5^\circ$  step size, PRF=14,400 Hz) was developed to acquire ultrafast ultrasound data at a compounded frame rate of 800 Hz. A 31.25-MHz, 1.5 cycle pulse was generated by the ultrasound system as the transmit signal. Each acquisition has 1280 14-bit quantization samples in fast time with a sampling frequency of 125 MHz (interleave sampling mode was used). The ultrasound data were transferred to a host computer (Dell Precision 5860 with Intel Xeon W7-2595X and 512 GB DDR5 RAM) via PCI-Express Gen3 x16 interface and stored to a NVME SSD array (RAID 0 with 4x Samsung 990 Pro 4TB). 1,920 compounded frames were acquired for each imaging plane (2.4 seconds acquisition for each imaging

plane). The imaging array was fixed on a motorized stage to translate in elevational direction with a step size of 60  $\mu\text{m}$ .

Rabbit kidney imaging: A Verasonics Vantage 256 standard-frequency configuration ultrasound imaging research platform that has 256 channels was used with a VisualSonics MS200 linear array that has 256 elements and a center frequency of 15 MHz. All elements of the probe were used to enable a field-of-view that has a width of 32 mm. An ultrafast plane-wave imaging sequence (9 titled plane waves,  $-4^\circ$  to  $4^\circ$  in  $1^\circ$  step size, pulse-repetition frequency PRF=33,333 Hz) was developed to acquire ultrafast ultrasound data at a compounded frame rate of 1852 Hz. 300 compounded frames were acquired (162 milliseconds). A pair of 10.83-MHz full cycle pulses with opposite polarity were generated by the ultrasound system for each steering angle and the received signals from both pulses were accumulated inside the Verasonics system to enable pulse inversion and reduce the data size. Each acquisition has 1664 14-bit quantization samples in fast time with a sampling frequency of 62.5 MHz. The ultrasound data were transferred to a host computer (Dell Precision 5820 with Intel Xeon W-2255 and 128 GB DDR4 RAM) via PCI-Express Gen3 x16 interface and stored to a NVME SSD (WD AN1500 1TB).

**Phase subtraction imaging.** After the acquisition of ultrafast ultrasound data, the reconstruction of label-free super-resolution microvessel image was performed using the phase subtraction imaging (PSI) algorithm. The PSI process is composed of three steps which are beamforming, clutter filtering, and phase subtraction.

For the beamforming, the ultrasound channel data are delayed and summed with three sets of weights that are also used in the null subtraction imaging (NSI) [6]. Three samples are beamformed at each pixel location following the process below:

$$\begin{bmatrix} S_{zm} \\ S_{dc1} \\ S_{dc2} \end{bmatrix} = [\mathbf{W}_{zm} \quad \mathbf{W}_{dc1} \quad \mathbf{W}_{dc2}]^T [\mathbf{R}_{delayed} \quad \mathbf{R}_{delayed} \quad \mathbf{R}_{delayed}]$$

where  $S_{zm}$ ,  $S_{dc1}$  and  $S_{dc2}$  are the three beamformed samples,  $\mathbf{W}_{zm}$ ,  $\mathbf{W}_{dc1}$  and  $\mathbf{W}_{dc2}$  are the three weight column vectors used in NSI, and  $\mathbf{R}_{delayed}$  is a column vector that contains delayed data samples across the subaperture. A fixed f-number of 1 was used to determine the subaperture size for beamforming samples at different depths. The beamformed samples at the same pixel location across different titled angles are summed together for coherent compounding. The same process was repeated for each pixel location and each frame to finish the ultrafast ultrasound beamforming.

For the clutter filtering, the beamformed data were first IQ demodulated and decimated to reduce the data size. Then, a singular value decomposition (SVD) based clutter filter was performed on the IQ data to filter out the static tissue signal and keep the native

blood flow signal. The spatiotemporal data matrix was formed in the same way as NSI power Doppler [5].

After the clutter rejection, the phase subtraction is performed following the process below:

$$\begin{aligned}
 P_1 &= \sum_{n=1}^{nf-1} \arg(\check{S}_{dc1}^n * (-\check{S}_{dc2}^{n+1})^*) \\
 P_2 &= \sum_{n=1}^{nf-1} \arg(\check{S}_{dc2}^n * (-\check{S}_{dc1}^{n+1})^*) \\
 P_3 &= \sum_{n=1}^{nf-1} \arg(\check{S}_{dc1}^n * (\check{S}_{zm}^{n+1})^*) \\
 P_4 &= \sum_{n=1}^{nf-1} \arg(\check{S}_{dc2}^n * (-\check{S}_{zm}^{n+1})^*) \\
 P_{PREA} &= (P_1 + P_2) \\
 P_{PREB} &= (P_3 + P_4) \\
 P_{PSI} &= P_{PREB} - P_{PREA}
 \end{aligned}$$

Where  $nf$  is the number of frames within one data set and  $n$  is the frame index.

$P_{PREA}$  and  $P_{PREB}$  are the two precursors of  $P_{PSI}$ . The final images are generated by accumulating  $P_{PSI}$  through all the frames acquired on the same imaging plane.

**Data Processing.** The data processing was performed on an ASUS ESC4000A-E12P server (AMD EPYC 9554 64-core processor, 768 GB DDR5 RAM and two NVIDIA RTX 6000 Ada GPUs) and accelerated on GPUs by Matlab `gpuArray` function. The voxel size was 4.5  $\mu\text{m}$  in lateral direction and 12.32  $\mu\text{m}$  in axial direction for 50-MHz imaging, 6.6  $\mu\text{m}$  in lateral direction and 12.32  $\mu\text{m}$  in axial direction for 30 MHz imaging, and 7.8125  $\mu\text{m}$  in lateral direction and 24.64  $\mu\text{m}$  in axial direction for rabbit kidney image. The first 10 percent and last 10 percent of the singular values were rejected to remove the static tissue and noise from the data. A fixed DC offset at 0.32 was selected empirically for the weights used in the beamforming. The volumetric visualization was rendered with Amira 2024.2.

**Measurement.** To provide a measurement that is localized for each vessel, auto skeletonization was performed using Matlab function `bwskel` and the microvessel radius was measured by finding the minimum Euclidean distance between a voxel on the

skeletonized vessel to the voxel that has half value of itself, i.e., a full width at half maximum (FWHM).

The improve ratio was calculated in a global manner. The 2D spatial frequency was calculated for each slice. Then the cut off amplitude was selected by finding the amplitude of CFI images at a spatial frequency at the inverse of one wavelength. The improvement ratio was then calculated by dividing the inverse of one wavelength with the corresponding spatial frequency of PSI images at the cut off amplitude.